This is the peer-reviewed, final accepted version for American Mineralogist, published by the Mineralogical Society of America.
The published version is subject to change. Cite as Authors (Year) Title. American Mineralogist, in press.
DOI: https://doi.org/10.2138/am-2023-8956. http://www.minsocam.org/

REVISION I

Znucalite, the only known zinc uranyl carbonate: its crystal structure and environmental implications

GWLADYS STECIUK[1], JURAJ MAJZLAN[2], JAN ROHLÍČEK[1], RADEK ŠKODA[3], JIŘÍ SEJKORA[4] AND JAKUB PLÁŠIL[1§]

[1] Institute of Physics of the CAS, Na Slovance 1999/2, 18200 Prague 8, Czech Republic

[2] Institute of Geosciences, Friedrich-Schiller University, Burgweg 11, Jena, 07749, Germany

[3] Department of Geological Sciences, Faculty of Science, Masaryk University, Kotlářská 2, 611 37, Brno, Czech Republic

[4] Department of Mineralogy and Petrology, National Museum, Cirkusová 1740, 193 00 Praha 9-Horní Počernice, Czech Republic

ABSTRACT

Znucalite is a zinc uranyl-carbonate that was until recently only partially characterized with a formula originally given as $Zn_{12}Ca(UO_2)(CO_3)_3(OH)_{22}\cdot 4H_2O$, with an unknown crystal structure and ambiguous symmetry determinations. We have reinvestigated this mineral using 3-dimensional electron diffraction (3D ED) and powder X-ray diffraction and revealed for the first time its structural details. Znucalite is unambiguously monoclinic, $P2_1/m$, with a = 10.722(2) Å, b = 6.259(1) Å, c = 25.355(1) Å, β = 101.13(1)º and V = 1669.54(9) Å^3. The structure refinement of the 3D ED data using the dynamical approach (R_{obs} = 0.1594 for 3579 observed reflections and 244 parameters) provided the following structure model. Znucalite possesses a layered structure, with a $[Zn_{10}(OH)_{14}(CO_3)_2]$ double sheet (with Zn^{2+} both in octahedra and tetrahedra), which is connected to a thick interlayer that hosts U^{6+}, Ca^{2+}, and H_2O molecules. The linkage between structural units and the interlayer occurs *via* the vertices of ZnO_4 tetrahedra protruding from the

§ Email: plasil@fzu.cz

sheet. In the interlayer, differences in ordering between U and Ca take place and likely caused the difficulties encountered during the attempts to solve the structure. The refined structural formula of znucalite, $Zn_{10}Ca_{0.828}[UO_2]_{0.828}[CO_3]_4(OH)_{15.312}(H_2O)_{5.484}$, corresponds well to the composition obtained from the electron-microprobe analyses, $(Zn_{9.84}Al_{0.16})_{\Sigma 10.00}Ca_{0.83}(UO_2)_{0.80}[(CO_3)_{3.96}(SO_4)_{0.04}]_{\Sigma 4.00}(OH)_{15.42}(H_2O)_{5.48}$. Raman spectroscopy evidenced the presence of several non-equivalent CO_3 groups, as well as OH and H_2O. The U–O bond lengths obtained from the stretching frequencies of UO_2^{2+} vibrations are in line with the structural model. A discussion on the environmental importance of znucalite is appended, based on geochemical calculations with an estimate of the solubility product for this mineral.

Keywords: znucalite, uranyl carbonate, crystal structure, 3D electron diffraction, Rietveld refinement, conditions of formation, uranium immobilization.

INTRODUCTION

Znucalite is the only uranyl carbonate containing zinc as an essential constituent. It was first described from the waste dump of the Lill mine in the Březové hory base-metal deposit in Příbram, Central Bohemia, Czech Republic (Ondruš et al. 1990). The description of the new mineral was based on powder X-ray diffraction data as znucalite from the type locality forms only powdery aggregates and efflorescences on the gangue deposited as mining waste in the old dump. Ondruš et al. (1990) reported the mineral to be triclinic and determined that its chemical formula is $Zn_{12}Ca(UO_2)(CO_3)_3(OH)_{22} \cdot 4H_2O$. Later on, Chiappero and Sarp (1993) reported on a new znucalite occurrence from the Mas d'Alary uranium deposit in Lodève (France). Based on the precession X-ray diffraction, they inferred znucalite to be orthorhombic and, thus, following

the density change, having a different formula from the original one, $Zn_{11}Ca(UO_2)(CO_3)_3(OH)_{20}\cdot 4H_2O$. Since then, znucalite has been reported from a few other localities worldwide. Nevertheless, since the work of Chiappero and Sarp (1993), no additional detailed crystallographic study has been undertaken, and the structure of znucalite remained unknown. Here we report on the first determination of the crystal structure of znucalite based on 3-dimensional electron diffraction (3D ED) techniques and Rietveld refinement from powder X-ray diffraction data.

ZNUCALITE OCCURRENCE IN JÁCHYMOV (CZECH REPUBLIC)

The znucalite occurrence in Jáchymov has been first reported by Ondruš et al. (1997) from the Jan Evangelista and Ondřej veins within the Svornost mine. The original material was discovered and collected in the 1980s. Nevertheless, we found the site as the detailed information was communicated to us by the late Jan Hloušek. Fortunately, his brief description helped us find the site and collect the samples directly in underground spaces. Thus, all solid and liquid samples used in this study come from the Jan Evangelista vein (the south mining field nearby the crossing with Ondřej vein) at the so-called Adit level of the Svornost mine in Jáchymov. The Jan Evangelista is one of the "midnight" veins (with NW–SE strike) and was one of the most economically important veins at this Bi-Co-Ni-Ag-U deposit. After World War II, it was intensively exploited for its U mineralization (Škácha et al. 2019). The vein is hosted by albitized Variscan biotite and biotite-phlogopite schists with lenses of calc-silicate rocks.

At the site studied, primary minerals in the vein are mostly calcite and dolomite, with a minor amount of quartz. No primary uraninite or sulfide minerals were observed. Znucalite at this site forms pseudo-speleothems in the mining gallery in a short interval of about 10–15 m. It

forms stalactites and curtains (with a thickness of up to 1 cm) on the ceiling and side walls of the gallery. On fractures, cracks, and edges, an unaided eye can recognize that znucalite forms crystalline aggregates, mostly globular, composed of usually bent, very thin elongated tabular crystals up to 80 μm in length (Fig. 1). Aggregates have pale yellow to off-white color and exhibit a yellowish green fluorescence when exposed to short- and long-wave UV radiation. Additional supergene minerals identified in the association (by powder X-ray diffraction) are gypsum and hydrozincite. Gypsum forms needle-like crystals growing in cavities along with znucalite. We have sampled the aqueous solutions dripping from the znucalite stalactites and curtains. The solutions were collected into syringes and filtered through 0.2 μm hydrophilic polypropylene filters. The volume of the samples rarely exceeded 5 mL and was insufficient for CO_2(aq) determination in the field. Temperature and pH were determined in the field on these aqueous solutions with a WTW multimeter with combined pH (SenTix 41, WTW, Germany) and ORP electrodes (SenTix ORP, WTW, Germany). It was assumed that pH and ORP values were not influenced by filtering and only filtered samples were subjected to these measurements. Before the measurements and regularly during the readings, pH was calibrated by standard solutions with buffers PL 2 (pH 1.68), PL4 (4.006), and PL 7 (6.865). The performance of the Ag/AgCl ORP electrode was checked regularly by measurements of Zobell's solution. The aqueous samples were diluted and split into two aliquots in the laboratory. One was acidified by ultrapure HNO_3; the other one was used without modifications to analyze anions. The concentration of selected ions was measured by a combination of inductively-coupled plasma (ICP) optical emission spectrometry (OES), ICP mass spectrometry (MS), or ion chromatography (IC). The instruments used were: an X-Series II, ThermoFisher Scientific (ICP-MS, Jena), and a radial Varian 725 OES (ICP-OES, Jena). Anions and selected cations were also analyzed by IC

systems DX120 (Dionex, Germany) (anion branch) with an AS40 autosampler (Jena). The elemental composition of the aqueous solutions sample from the Jan Evangelista vein (Znuk) is given in Table 1.

CHEMICAL COMPOSITION

The chemical composition of znucalite was determined from the polished and carbon-coated fragments mounted in an epoxy cylinder using a Cameca SX 100 electron microprobe. The instrument was operated in a wavelength-dispersive mode at an accelerating voltage of 15 kV, beam current of 5 nA, and beam diameter of 20 μm. The following X-ray lines and standards were selected; *K*α lines: Al (sanidine), Ca (fluorapatite), S (celestine), Zn (ZnO), and *M*α line: U (UO_2). Other elements with Z > 8 were sought but were below detection limits (~0.05–0.10 wt.%). Counting times were 10–20 s on peak and half of this time for each background position. The raw intensities were converted to oxide concentrations automatically using *PAP* (Pouchou and Pichoir 1985) matrix correction software. Water and CO_2 could not be analyzed directly because of the very small amount of material available; their presence was confirmed by Raman spectroscopy and calculated based on the proposed structural formula and charge balance. Analytical data for znucalite are given in Table 2. In addition to Zn, Ca and U, the studied sample contains minor amounts of Al (up to 0.31 *apfu*) and S (up to 0.10 *apfu*). The contents of Al negatively correlate with Zn. No correlation between Al and Ca was observed. The empirical formula of znucalite from Jáchymov (mean of 20 spot analyses), calculated based on **(**Zn+Al) = 10 *apfu***,** is: $(Zn_{9.84}Al_{0.16})_{\Sigma 10.00}Ca_{0.83}(UO_2)_{0.80}[(CO_3)_{3.96}(SO_4)_{0.04}]_{\Sigma 4.00}(OH)_{15.42}(H_2O)_{5.48}$.

RAMAN SPECTROSCOPY

The Raman spectra of znucalite were collected in the range 20-4000 cm^{-1} using a DXR dispersive Raman Spectrometer (Thermo Scientific) mounted on a confocal Olympus microscope. The Raman signal was excited by an unpolarised 532 nm solid state, diode-pumped laser, and detected by a CCD detector. The experimental parameters were: 100× objective, 10 s exposure time, 100 exposures, 50 μm pinhole spectrograph aperture, and 10 mW laser power level. The eventual thermal damage of the measured points was excluded by visual inspection of the excited surface after measurement, observation of possible decay of spectral features at the start of excitation and checking for thermal downshift of Raman lines. The instrument was set up by a software-controlled calibration procedure using multiple neon emission lines (wavelength calibration), multiple polystyrene Raman bands (laser frequency calibration) and standardized white-light sources (intensity calibration). Spectral manipulations were performed using the Omnic 9 software (Thermo Scientific).

The Raman spectrum of znucalite is dominated by bands connected to vibrations of carbonate, uranyl and H_2O/OH groups (Fig. 2). A broad set of bands in the region 3700 - 3000 cm^{-1} with maxima at 3662, 3590, 3510, 3382 and 3265 cm^{-1} are assigned to ν O–H stretching vibrations of structurally non-equivalent OH groups and water molecules bonded in the crystal structure by the network of H-bonds. According to the empirical relation provided by Libowitzky (1999), the approximate O–H···O hydrogen bond lengths inferred from the observed stretching frequencies lie within the range >3.2 to 2.7 Å. The weak bands at 2970 and 2912 cm^{-1} correspond to bond lengths of 2.66–2.67 Å. A band observed at 1653 cm^{-1} is attributed to the ν_2 (δ) H–O–H bending vibrations of water molecules. Raman bands at 1596, 1551, 1403 and 1372 cm^{-1} are related to the split doubly degenerate ν_3 $(CO3)^{2-}$ antisymmetric stretching vibrations; observed splitting indicates the presence of bidentate-bonded carbonate groups onto uranyl hexagonal

bipyramids in the crystal structure (Jolivet et al. 1980; Čejka 1999). Raman bands at 1082 and 1061 cm^{-1} are attributed to the ν_1 $(CO_3)^{2-}$ symmetric stretching vibrations. The number of bands proves that symmetrically distinct $(CO_3)^{2-}$groups are present in the structure. A particularly strong Raman band at 843 cm^{-1} is related to the ν_1 $(UO_2)^{2+}$ symmetric stretching vibration. The approximate U–O bond length inferred from the observed wavenumber assigned to this vibration of about 1.77 Å (empirical relation of Bartlett and Cooney 1989), which is comparable with the U–O bond length of 1.779 Å found in the crystal structure analysis. Raman bands at 772, 743, and 711 cm^{-1} are assigned to the split doubly degenerate ν_4 (δ) $(CO_3)^{2-}$ in-plane bending vibrations. Very weak Raman bands at 532 and 510 cm^{-1} can be related to the libration modes of water molecules. The character of the Raman spectrum in the region 400–200 cm^{-1} with bands 430, 384, 352, 281, and 221 cm^{-1} is comparable with bands found in the Raman spectrum of synthetic hydrozincite (Hales and Frost 2007); we expect these bands are most likely connected with vibrations of bonds of the ZnO_4 tetrahedra and ZnO_6 octahedra. Raman bands at 281 and 221 cm^{-1} may partly coincide with the doubly degenerate ν_2 (δ) $(UO_2)^{2+}$ bending vibrations. The remaining Raman bands at 151, 96 and 31 cm^{-1} are assigned to lattice vibrations.

CRYSTAL STRUCTURE

Single-crystal X-ray diffraction

A crystal of znucalite of approximate dimensions 0.038 × 0.022 × 0.010 mm was chosen from an oil suspension in a polarized-light microscope, mounted on a thin glass fibre and examined at room temperature with a Rigaku SuperNova X-ray single-crystal diffractometer equipped with the Atlas S2 CCD detector and a microfocus MoKα source. Even though the crystal was weakly diffracting, the diffraction spots were sharp and the preliminary unit cell obtained from this experiment was deemed reasonable. A full-sphere data collection was undertaken with a

164 relatively long counting time (400 seconds per 1°) and a high-sensitivity mode of the Atlas
165 detector (4×4 px and high gain). Nevertheless, it resulted in a poor data set, with an R_{int} of 31%
166 for the *mmm* Laue class. Careful inspection of diffraction frames revealed that the crystal was
167 split and consisted of at least two similarly diffracting domains (regarding their intensities),
168 anisotropic profiles, and smeared diffraction streaks. Subsequent trials to obtain partial but
169 reasonable structure solution from these data failed. However, a (pseudo-orthorhombic)
170 monoclinic unit cell obtained from the profile fitting of 1021 observed reflections, with a =
171 5.3807(16) Å, b = 6.3273(13) Å, c = 25.129(12) Å, β = 90.59(3)º with V = 855.5(5) Å^3 was later
172 found to represent a sub-cell of the real (ordered) structure related to the disordered model. As the
173 quality of all other tested crystals was similar or worse, we decided to utilize 3D electron
174 diffraction to reveal the structure (see below).
175
176 *Powder X-ray diffraction and Rietveld refinement*
177 Znucalite crystals were mildly ground under acetone and placed in a 0.5 mm borosilicate-glass
178 capillary for X-ray powder diffraction (XRPD) data. Data were collected using the Debye-
179 Scherrer transmission configuration on the powder diffractometer Empyrean of PANalytical (λ =
180 1.54184 Å) equipped with a focusing Göbel mirror, capillary holder, and PIXcel3D detector.
181 The 20-hour measurement was undertaken from 3 to 80 °2θ with 0.013° step size and 6000 s per
182 step at ambient temperature. LeBail fitting and a subsequent Rietveld refinement were done in
183 Jana2020 (Petříček et al. 2020).
184
185 *3D ED data collection*

For TEM analysis, we used znucalite, which forms aggregates composed of folded, very thin tabular crystals up to a few μm in length. Clusters of crystals were gently crushed and deposited without solvent on a Cu-grid coated by a thin film of holey amorphous carbon. The 3-dimensional electron diffraction (3D ED) data were collected with two different transmission electron microscopes (TEM) and detectors. The first 3D ED series of datasets were collected using a Philips CM120 TEM (acceleration voltage of 120 kV, LaB_6) equipped with a side-mounted CCD camera Olympus Veleta with a 14-bit dynamic range. Additional data sets were acquired more recently with an FEI Tecnai 02 transmission electron microscope (TEM) (acceleration voltage of 200 kV, LaB_6) equipped with a side-mounted hybrid single-electron detector ASI Cheetah M3, 512 × 512 pixels with high sensitivity and a fast readout. To preserve the hydrated structure of the mineral under the high vacuum in the instrument, the grids were plunged into liquid nitrogen and transferred to the TEM using a Gatan cryo-transfer holder. The precession electron diffraction tomography (PEDT) technique was chosen (Gemmi and Lanza 2019) to further reduce the dynamical effects, using the precession device Nanomegas Digistar (Vincent and Midgley 1994) and a precession semi-angle of 1°. Data sets were collected at 100 K on several single crystals in stepwise mode with the tilt step of the goniometer set to 1° (Fig. 3). To limit the beam-induced damage to the crystals, low illumination settings were used. 3D ED data reduction was performed using the computer program PETS2 (Palatinus et al. 2019; Brázda et al. 2022). The structural analysis mainly relies on two 3D ED data sets, which present the most ordered stacking associated with the lowest apparent mosaicity of the crystals (Fig. 4). For each 3D ED data set, the data reduction yielded two *hkl*-type files: one assuming the kinematical approximation (for structure solution and the so-called kinematical refinement) where reflections are merged, and a second used for the dynamical refinement where all frames of the data set are

209 independently refined. Two data sets were merged in JANA2020 for the structure solution to
210 increase the data coverage up to 83% (Palatinus et al. 2015). The structure was solved using
211 Superflip (Palatinus and Chapuis 2007; Palatinus 2013) implemented in Jana2020 (Petříček et al.
212 2020) and refined using DYNGO and Jana2020. For the kinematical refinement, the two data
213 blocks were refined in parallel. Only one data (crystal #1) set from the most well-crystallized
214 crystal was found suitable for the dynamical refinement.
215
216 *Structure solution*
217 Data collected on znucalite are characteristic of a layered structure with smeared reflections
218 along the stacking direction *c,* which only affect every two rows along *a* (Fig. 3). A pseudo-
219 orthorhombic basic cell (a_0 = 5.361(2) Å, b_0 = 6.259(1) Å, c_0 = 25.304(1) Å, α ≈ β ≈ γ ≈ 90 º)
220 corresponds to the ordered part of the structure. However, the unit cell becomes distinctly
221 monoclinic when the additional rows of reflections $h = 2n+1$ are considered with parameters a =
222 $2a_0$ = 10.722(2) Å, $b = b_0$ = 6.259(1) Å, c = 25.355(1) Å, β = 101.13(1)º and V = 1669.54(9) Å^3.
223 The extinctions $k = 2n$ on $0k0$ indicates the space group $P2_1/m$, later confirmed in the Superflip
224 program and the XRPD data (Fig. 5). The additional row is a signature of ordering. The
225 intensities and diffuse character of the reflections $h = 2n+1$ along **c** vary from one crystal to
226 another (~ 15 data sets), which implies that the ordering is imperfect along the stacking direction,
227 and sometimes nearly absent (Fig. 3). The structure was solved *ab-initio* from two merged data
228 sets (kinematical approximation) with 83% completeness up to the resolution of sin(θ)/λ = 0.72
229 Å^{-1}. The completeness is limited due to the (001) preferred orientation of the crystals on the grid
230 and the incomplete rotation of the goniometer. The most important experimental parameters are
231 listed in Table 3. The initial solution was incomplete and described first as a fully ordered block

with Zn–O polyhedra and CO_3 groups, and secondly, one partially occupied uranium site in the thick interlayer bonded to ZnO_4 tetrahedra via two carbonate groups. The remaining structure of the interlayer was completed step by step from the difference-electrostatic potential maps (difference Fourier map for electron data) after the refinement of the initial structure. The missing non-hydrogen atoms are usually determined after the kinematical refinement, before obtaining more accuracy with the dynamical refinement of the complete structure. For znucalite, the kinematical refinement left the topology of the interlayer structure ambiguous and the dynamical refinement was directly applied to complete the model. Electron-diffraction data always suffer from dynamical effects (or multiple scattering), which break the kinematical approximation □$_{h}$□□ □ □$_{h}$□□^{2}. The so-called "kinematical refinement", which assumes the kinematical approximation leads to low structural accuracy and large figure of merit. Therefore, the dynamical theory must be considered to reach the finest structural details from 3D ED data. However, for poorly crystallized domains with smeared reflections, none of these two refinements can perfectly describe the data as they do not account for the scattering occurring out of the Bragg position. The refinement of znucalite, especially regarding the interlayer, is then limited by the presence of the diffuse $h = 2n+1$ reflections, the high mosaicity and the partial data completeness. Nonetheless, after a few refinement cycles of the initial model, the residual electrostatic potential map (difference Fourier map) could unveil the nature of the U/Ca ordering with the presence of partially occupied sites: one Ca, one additional CO_3 group around the uranyl group, the O sites to fulfill the Ca coordination and disordered H_2O molecules.

From our model and $Z = 2$, the formula is $Zn_{10}Ca_xU_x(CO_3)_y(OH+H_2O)$ (for water content, see below) with x and y, initially refined for values close to $x = 0.75$ and $y = 4$. From previous studies, znucalite has been described with the ideal formula $Zn_{12}(UO_2)Ca(CO_3)_3(OH)_{22}(H_2O)_4$,

but lacking a structural model (Ondruš et al. 1990). The Zn : U : Ca = 12 : 1 : 1 ratio corresponds to 10:0.828:0.828 in our model (Z = 2), and x was later set to 0.828 to follow the ratio obtained from the electron microprobe analysis. The occupancies of the oxygen sites in the interlayer were set according to the bonded cations (Ca or U), and the overall CO_3 content was set to 4 with C3 fully occupied and (C4+C5) fully occupied. The bond-valence analysis of the oxygen sites belonging to the dense layer showed that all oxygen sites labeled from O1 to O10 are, in fact, hydroxyl groups (Table 4). The apical oxygen of the two ZnO_4 tetrahedra protruding from the Zn double layer is either part of a CO_3 group (O1c3, O1c4) or hydroxyl in the absence of C4 (O1c4-H) (Table 4). Several restrictions were applied on the cation–O distances and the atomic displacement parameters to stabilize the CO_3 groups and the configuration of the interlayer (see CIF file for the list). After only a few refinement cycles with the complete interlayer, the residual electrostatic potential map showed maxima above 2σ or 3σ [$\Delta V(r)$] corresponding to the ten expected hydrogen positions (OH) bonded to the oxygen atoms of the $[Zn_{10}(OH)_{14}(CO_3)_2]^{2+}$ block (Fig. 8). All O–H distances were restrained to 1.00 Å. The isotropic displacement parameters of hydrogen atoms were set as riding with an extension factor of 1.2 times that of the O to which they are bonded. The missing disordered interlayer H sites (partially occupied) could not be determined from our data. The final dynamical refinement led to R(obs)/wR(obs) = 0.1594/0.1720, R(all)/wR(all) = 0.3677/0.1888 for 3579/20304 observed/all reflections and 244 refined parameters. For comparison, the kinematical refinement gives R(obs)/wR(obs) = 0.3296/0.2620, R(all)/wR(all) = 0.3614/0.2681for 5564/7331 observed/all reflections. The R-values significantly decreased when the dynamical theory was applied; however, they remained higher than usual because of the imperfect ordering, especially for reflections h = 2n+1 (Table 3). The formula obtained from 3D ED is $Zn_{10}Ca_{0.828}(UO_2)_{0.828}(CO_3)_4(OH)_{15.312}(H_2O)_{5.484}$ with 14

hydrogens (of the OH groups) discernible from the data. Further refinement details are given in Table 3, interatomic distances in Table 5 and the bond valence analysis Table 6 and 7 (without and with hydrogen contribution). A representation of the znucalite structure is shown in Figures 7 and 8. The model obtained from 3D ED was used to perform a Rietveld refinement against the XRPD data. First, this allowed us to confirm the symmetry and the structure of znucalite in a bulk sample at ambient temperature and without the danger of dehydration of the sample. At ambient temperature, the lattice parameters are a = 10.7655(6) Å, b = 6.3291(2) Å, c = 25.5407(6) Å with β = 100.851(5)º. Secondly, at a larger scale in the bulk sample, the ordering of the interlayer appears less pronounced as the doubling of the a parameter characteristic of the ordering is very weak and gives broader peaks. From the structural perspective, the refined XRPD structural model is almost averaged with the O11 site that becomes a mixed site shared with uranium, as well as Ca1 with O (Fig. 8). This refinement converged toward R(obs)/wR(obs) = 0.0718/0.1063, R(all)/wR(all) = 0.0725/0.1063 for 1191/1195 observed/all reflections and 48 refined parameters. The profile parameters were R_p = 0.0622, wR_p = 0.0436 and GOF = 0.2451 (Table 3 and Fig. 9).

DESCRIPTION OF THE STRUCTURE

The structure of the main block $[Zn_{10}(OH)_{14}(CO_3)_2]^{2+}$ is described by eight independent Zn sites in the asymmetric unit cell (6× 2*e* and 2× 4*f*), *i.e.,* 10 Zn per unit cell (Z = 2). The double Zn layer contains two CO_3 groups (2× 2*e*) and ten additional O sites (4× 4*f* + 6× 2*e*), all fully occupied. Four Zn sites are in tetrahedral coordination (ZnO_4), and the last four form ZnO_6 octahedra with the 12 surrounding oxygen positions (Fig. 7). The ZnO_6 coordination octahedron has an average Zn–O distance of 2.110(8) Å (varying from 1.923(8) to 2.258(8) Å) and the average tetrahedral

Zn–O distance is 1.95(1) Å (1.863(11)-2.174(11) Å) (see Table 5 for individual polyhedra). The extended range of metal-oxygen distances is typical of Jahn-Teller distortions in Zn^{2+}. The occurrence of strongly distorted octahedra is fairly common in the crystal chemistry of zinc and was reported for related phases (Ghose 1964; Stählin and Oswald 1970; Harding et al. 1994; Gordeeva et al. 2020). The ratio of octahedral to tetrahedral zinc-centered polyhedra in the sheet structure thus formed is 3:2. The same ratio is found in hydrozincite, $Zn_5(CO_3)_2(OH)_6$ (Ghose 1964), the synthetic $Zn_5(OH)_{10}\cdot 2H_2O$ (Gordeeva et al. 2020), and $Zn_5(OH)_8(NO_3)_2\cdot 2H_2O$ (Stählin and Oswald 1970). All of those compounds possess a very similar Zn block. The single-layer of the $[Zn_{10}(OH)_{14}(CO_3)_2]^{2+}$ slab in znucalite with the formula $[Zn_5(OH_7)(CO_3)]^{1+}$ can be regarded as a variation of a hypothetical $Zn(OH)_2$ structure of the C6 or CdI_2 type, where one-quarter of the zinc atoms of $Zn(OH)_2$ structure is being removed from the sheet, and one-quarter of the hydroxyl groups is replaced by O^{2-}. Each occupied octahedron shares its edges with two unoccupied and four occupied octahedra (Fig. 7). The ZnO_6 polyhedra are connected to create a flat slab in the (*a,b*) plane with hexagonal cavities. The ZnO_4 tetrahedra occur above and below the vacant positions. The CO_3 groups appear first on one side of the single layer by the interstice, with one oxygen atom of the carbonate group being a part of the ZnO_6 octahedra. On the other hand, the CO_3 groups between the two layers are linked to ZnO_4 tetrahedra and uranyl groups and form the link between the two Zn layers. The second $[Zn_5(OH_7)(CO_3)]^{1+}$ layer is obtained by applying inversion. The carbonate groups lie on the mirror planes at *y* equal to ¼, or ¾, and hence are normal to the zinc sheets. Carbonate groups bind the dense sheets together in a three-dimensional network by sharing a vertex of the Zn tetrahedron pointing out of the sheet and a vertex of the Zn octahedron occurring in the sheet next above; the third corner is bonded with a strong hydrogen bond to one $(OH)^-$ group of the second layer and two $(OH)^-$ groups of the same

layer (Fig. 7). The complex sheet structure can also be described in terms of coordination polyhedra around zinc. Two parallel chains composed of $Zn(OH)_5(O)$ octahedra sharing common edges are running along [010]. These two chains are bridged by octahedra, sharing two edges with two octahedra of each chain. The connection is also facilitated above and below by the ZnO_4 tetrahedra that share two vertices with one chain and one with the other. So far, the description of znucalite structure is very close to that of hydrozincite (Ghose 1964). However, instead of the infinite stacking of the $Zn_5(OH)_6(CO_3)_2$ sheet, in znucalite the double-layer sheet $[Zn_{10}(OH)_{14}(CO_3)_2]$ is connected to a thick interlayer that hosts U^{6+}, Ca, and H_2O molecules through the vertices of the ZnO_4 tetrahedra sticking out of the slab above and below the sheet.

The uranium site is only partially occupied (s.o.f. = 0.828), and it exhibits a characteristic UO_8 hexagonal bipyramidal coordination centered on the linear uranyl $(UO_2)^{2+}$ ion. The refinement shows the signature of three possible CO_3 groups around UO_8, lying in the (010) plane, hence normal to the zinc sheets (C3, C4 and C5). However, the partial occupancies of C4 and C5 show that mainly only two CO_3 groups are present at the same time around the uranyl ion, and thus the uranyl tricarbonate complex, $[(UO_2)(CO_3)_3]^{4-}$, is nominally absent, (C4 + C5 = 1) (Fig. 8). Moreover, Raman spectroscopy combined with the results of the crystallographic analyses confirm the unusual presence of uranyl di-carbonate rather than uranyl-peroxo-di-carbonate. The UO_8 polyhedra are connected to the Zn block *via* two CO_3 groups, as shown in Figure 8. In the absence of CO_3 (C4), the apical oxygen of ZnO_4 tetrahedra (Zn8) becomes a hydroxyl group. The calcium in the interlayer (s.o.f. = 0.828) is connected to two oxygen sites which can be CO_3 groups or H_2O associated with the UO_8 polyhedra *via* vertices, as well as to four partially occupied and disordered H_2O molecules in a disordered pentagonal pyramidal coordination. Again, the pentagonal plane coincides with the (010) plane, as for the equatorial

plane of UO_8 and the CO_3 groups. The interlayer contains two additional disordered H_2O molecules (Ow1/Ow1b and Ow2/Ow2b). The difference-Fourier map of the interlayer remains noisy after the dynamical refinement, suggesting that it may contain additional H_2O molecules.

DISCUSSION

Crystal structure

The topology of the interlayer is mainly characterized by the ordering between uranyl di-carbonate and calcium along **a**. From single-crystal 3D ED data selected for the refinement, the ordering is complete and no significant trace of uranium is found in the O11 site (ignoring stacking faults). However, some crystals measured with 3D ED exhibit a much weaker row of h = 2n+1 reflections showing that in certain cases, the U/Ca ordering is nearly absent. The same observation is made from the XPRD data, where the few peaks associated with the ordering are weak, broader, and more asymmetric than the peaks of the basic cell. In that case, the partial ordering makes the structure of the interlayer difficult to interpret in detail with mixed sites U1/□, Ca/O, O11/□/U2, and O/□. In the extreme case of a crystal showing no ordering, *i.e.,* no doubling of the a_0 parameter, the structure of the interlayer becomes the superimposition of all possible configurations (see insert in Fig. 8). This conclusion explains why all attempts to solve the structure of the basic cell from 3D ED failed to describe the interlayer topology.

The ambiguity in the so far reported unit cells for znucalite, all based on X-ray powder diffraction data (Table 8), can be attributed to the weaker and imperfect $UO_2(OH)_2(CO_3)_2/Ca(H_2O)_4$ ordering. Our XPRD data are sharp enough to allow for an accurate comparison. A simple Le-Bail refinement from XPRD data using the different reported unit cells shows that the orthorhombic setting fails to model a few peaks in the diagram. However,

lowering the symmetry to a triclinic space group (Ondruš et al. 1990) is not necessary as the monoclinic unit cell determined from 3D ED with space group $P2_1/m$ gives the best description of the data. The pseudo-orthorhombic basic cell without U/Ca ordering with $a = a_0$ refines in fact as a monoclinic unit cell with parameters a_0 = 5.311(1) Å, b_0 = 6.3291(2) Å, c_0 = 25.099(1) Å, β = 92.032(1)º. From 3D ED, the β angle of the basic cell was not significantly different from 90º to detect a monoclinic deformation. Other phases with a similar topology of the Zn slabs, like hydrozincite, $Zn_5(OH)_6(CO_3)_2$, aurichalcite $(Cu,Zn)_5(OH)_6(CO_3)_2$, and synthetic $Zn_5(OH)_{10}\cdot 2H_2O$ and $Zn_5(OH)_8(NO_3)_2\cdot 2H_2O$, all have monoclinic symmetry, very similar to the parameters of the znucalite basic cell (without ordering) or the monoclinic unit cell (with ordering) of znucalite, except stacking parameters (Table 8).

In hydrozincite, a related mineral, the single Zn single layers are similar, but they are covalently bonded to each other and do not present specific stacking disorder. However, the usual corrosion product of zinc in moist air is a stacking-disordered phase of hydrozincite (Ghose 1964), where the resulting thin coating protects the metal from further corrosion. In nature, it occurs in the oxidation zone of ore deposits as an alteration product of sphalerite, usually as earthy masses, rarely as thin needle-shaped crystals. Since the carbonate groups hold the complex sheets together, replacing some carbonate groups with OH ions will facilitate random mistakes in the layer sequence giving rise to more disordered phases. It is also reported that the natural aging process with CO_2 reconstitutes the structure and leads to more ordered stacking (Ghose 1964). In znucalite, the adjacent Zn single layers are held together by hydrogen bonds from carbonate oxygen to hydroxyl groups like in aurichalcite (Harding et al. 1994) and the corrosion product of Zn. However, the hydrogen bonding between Zn layers in znucalite is not the origin of the observed stacking disorder and the stacking of the two adjacent Zn slabs is the most ordered part

of the structure (sharp reflections related to the sub-lattice). Therefore, the stacking faults are rather driven by the imperfect U/Ca ordering in the interlayer which is illustrated in the diffraction pattern by diffuse h = 2n+1 reflections along **c** (Figure 3).

ENVIRONMENTAL IMPLICATIONS

The studied site where znucalite currently forms provided unique data to clarify its formation and stability. The aqueous solution from which znucalite precipitates has circumneutral pH and high oxidation-reduction potential. Calculation of saturation indices with the program PHREEQC shows that the solution is essentially in equilibrium with gypsum and chalcedony. This result agrees well with the observation that gypsum is associated with znucalite in the mine gallery and the Si-rich phase is locally present in znucalite aggregates studied by electron microprobe. Slight supersaturation with respect to ferrihydrite is unusual because it is most likely the consequence of analytical difficulties with near-neutral solutions with very little Fe. In agreement, the znucalite speleothems are free of iron-oxide stains, otherwise omnipresent in the mine.

High concentrations of zinc ($1–7\times10^{-4}$ molal) and traces of uranium ($1–3\times10^{-6}$ molal) lead to rapid precipitation of znucalite. We were not able to measure carbonate concentrations in the aqueous solutions. There are no signs, however, that these solutions are supersaturated with respect to calcite. Calcite was not found together with znucalite. We assume, therefore, that the solutions are in equilibrium with CO_2(gas) in the air. Calculations with this assumption confirm the undersaturation with respect to calcite (SI of ~ –2). The solutions are also undersaturated with respect to hydrozincite (SI of –3), a phase structurally close to znucalite. If the solution is assumed to be in equilibrium with respect to znucalite under these conditions, then log K_{sp} for the reaction

414 $Zn_{10}Ca_{0.828}(UO_2)_{0.828}(CO_3)_4(OH)_{15.312}\cdot 5.484H_2O + 19.312H^+ \rightarrow 10Zn^{2+} + 0.828Ca^{2+} + 0.828$
415 $(UO_2)^{2+} + 4HCO^{3-} + 20.796H_2O$

416 is approximately +67. We can assume that it is not a coincidence that the proportions of U and
417 Ca are so close in znucalite. This might also indicate that a ~Ca-$U(CO_3)_2$ complex is present in
418 solution or that some multistep rearrangement/hydrolysis/decarboxylation, of a tricarbonate
419 species contributes to the disorder. Moreover, it is interesting to speculate that the "znucalite"
420 from France (Chiappero and Sarp 1993), or even Ondruš material (Ondruš et al. 1990), could
421 actually represent other species with variable Zn, OH, and uranyl tri or dicarbonate. We consider
422 znucalite and disordered hydrozincite-like phases to be important agents to remove U from the
423 groundwater locally.

424 **ACKNOWLEDGMENTS**

425 The comments by Travis Olds and Fernando Camara helped us to improve the manuscript. This
426 work was primarily financially supported by the Czech Science Foundation (GACR 20-11949S)
427 and the CzechNanoLab Research Infrastructure supported by MEYS CR (LM2018110). We also
428 want to acknowledge the support of the Operational Programme Research, Development and
429 Education financed by European Structural and Investment Funds and the Czech Ministry of
430 Education, Youth and Sports (Project No. SOLID21 CZ.02.1.01/0.0/0.0/16_019/0000760) and
431 the OP VVV project (Geobarr CZ.02.1.01/0.0/0.0/16_026/0008459 to RS) and by the Ministry of
432 Culture of the Czech Republic (long-term project DKRVO 2019–2023/1.II.e; National Museum,
433 00023272) to JS.

434 We dedicate this paper to the memory of our colleague and friend, the late Dr. Jan Hloušek
435 (1950–2014), who first found znucalite in Jáchymov and drew our attention to that particular
436 occurrence.

REFERENCES

Bartlett, J.R. and Cooney, R.P. (1989) On the determination of uranium-oxygen bond lengths in dioxouranium(VI) compounds by Raman spectroscopy. Journal of Molecular Structure, 193, 295–300.

Brown, I.D. (2002) The chemical bond in inorganic chemistry: the bond valence model. Oxford University Press, UK, 1–278.

Brázda, P., Klementová, M., Krysiak, Y., and Palatinus, L. (2022) Accurate lattice parameters from 3D electron diffraction data. I. Optical distortions. IUCrJ, 9, 1–21.

Čejka, J. (1999) Infrared spectroscopy and thermal analysis of the uranyl minerals. Reviews in Mineralogy and Geochemistry 38, 521–622

Chiappero, P.J., and Sarp, H. (1993) Nouvelles données sur la znucalite et seconde occurrence: Le Mas d'Alary, Lodève (Hérault, France). Archives des Sciences, Genève, 46, 291–301

Gagné, O.C., and Hawthorne, F.C. (2015) Comprehensive derivation of bond-valence parameters for ion pairs involving oxygen. Acta Crystallographica, B71, 562–578.

Gemmi, M., and Lanza, A. E. (2019) 3D electron diffraction techniques. Acta Crystallographica B, 75, 495–504.

Ghose, S. (1964) The crystal structure of hydrozincite, $Zn_5(OH)_6(CO_3)_2$. Acta Crystallographica, 17, 1051–1057.

Gordeeva, A., Hsu, Y.J., Jenei, I.Z., Brant Carvalho, P.H.B., Simak, S.I., Andersson, O., and Haüssermann, U. (2020) Layered Zinc Hydroxide Dihydrate, $Zn_5(OH)_{10}\cdot 2H_2O$, from Hydrothermal Conversion of ϵ-$Zn(OH)_2$ at Gigapascal Pressures and its Transformation to Nanocrystalline ZnO. ACS Omega, 5, 17617–17627.

459 Hales, M.C. and Frost, R.L. (2007) Synthesis and vibrational spectroscopic characterisation of
460 synthetic hydrozincite and smithsonite. Polyhedron, 26(17), 4955-4962.

461 Harding, M.M., Kariuki, B.M., Cernik, R. and Cressey, G. (1994) The structure of aurichalcite,
462 $(Cu,Zn)_5(OH)_6(CO_3)_2$, determined from a microcrystal. Acta Crystallographica B, 50, 673–
463 676.

464 Jolivet, J.P., Thomas, Y., Taravel, B. (1980) Vibrational study of coordinated CO_3^{2-} ions. Journal
465 of Molecular Structure, 60, 93–98

466 Libowitzky, E. (1999) Correlation of O–H stretching frequencies and O–H···O hydrogen bond
467 lengths in minerals. Monatshefte für Chemie, 130, 1047–1059.

468 Ondruš, P., Veselovský, F., and Rybka, R. (1990) Znucalite, $Zn_{12}(UO_2)Ca(CO_3)_3(OH)_{22}.4H_2O$, a
469 new mineral from Příbram, Czechoslovakia. Neues Jahrbuch für Mineralogie, Monatshefte,
470 9, 393–400.

471 Ondruš, P., Veselovský, F., Hloušek, J., Skála, R., Vavřín, I., Frýda, J., Čejka, J. and Gabašová,
472 A. (1997). Secondary minerals of the Jáchymov (Joachimsthal) ore district. Journal of the
473 Czech Geological Society, 42(4), 3–76.

474 Palatinus, L. (2013) The charge-flipping algorithm in crystallography. Acta Crystallographica B,
475 69, 1–16.

476 Palatinus, L., and Chapuis, G. (2007) SUPERFLIP – a computer program for the solution of
477 crystal structures by charge flipping in arbitrary dimensions. Journal of Applied
478 Crystallography, 40, 786–790.

479 Palatinus, L., Corrêa, C.A., Steciuk, G., Jacob, D., Roussel, P., Boullay, P., Klementová, M.,
480 Gemmi, M., Kopeček, J., Domeneghetti, M.C., and others (2015) Structure refinement

using precession electron diffraction tomography and dynamical diffraction: tests on experimental data. Acta Crystallographica Section B Structural Science, Crystal Engineering and Materials, 71, 740–751.

Palatinus, L., Brázda, P., Jelínek, M., Hrdá, J., Steciuk, G., and Klementová, M. (2019) Specifics of the data processing of precession electron diffraction tomography data and their implementation in the program PETS2.0. Acta Crystallographica B, 75, 512–522.

Petříček, V., Dušek, M., and Palatinus, L. (2020) Crystallographic computing system Jana2020. Institute of Physics, CAS, Prague, Czech Republic.

Pouchou, J.L., and Pichoir, F. (1985) "PAP" (πρZ) procedure for improved quantitative microanalysis. In J.T. Armstrong, Ed., Microbeam Analysis, p. 104–106. San Francisco Press, California.

Stählin, W., and Oswald, H.R. (1970) The crystal structure of zinc hydroxide nitrate, $Zn_5(OH)_8(NO_3)_2.2H_2O$. Acta Crystallographica Section B Structural Crystallography and Crystal Chemistry, 26, 860–863.

Škácha, P., Plášil, J. and Horák, V. (2019) Jáchymov – mineralogická perla Krušnohoří. Academia, Praha, pp 1–688 (in Czech with English Summary).

Vincent, R., and Midgley, P. A. (1994) Double conical beam-rocking system for measurement of integrated electron diffraction intensities. Ultramicroscopy, 53, 271–282.

Figures

FIGURE 1 The group of bent very thin tabular crystals of znucalite, BSE photo.

FIGURE 2 Raman spectrum of znucalite (split at 2000 cm^{-1}).

FIGURE 3 from left to right: picture of the two most ordered crystals used in the structural analysis and sections of the reciprocal space showing the quality of the stacking along **c*** in crystal #1, and in another less ordered crystal (labeled #3). The purple rings on the sections correspond to the 1 $Å^{-1}$ resolution.

FIGURE 4 Plots of the rocking curve profiles (Camel plot) of the experimental 3D ED data collected on the two most ordered crystals. For each data set, rocking curves are given by resolution shell for reflections with $I \geq 10\sigma(I)$. The lowest blue curve is the averaged observed RC in the range 0.2 to 0.3 $Å^{-1}$ and the next curves are obtained by steps of 0.1 $Å^{-1}$. The red curve corresponds to the calculated curve.

FIGURE 5 LeBail refinements of znucalite from X-ray powder data using the two reported settings: triclinic (Ondruš et al. 1990) (blue), and orthorhombic (Chiappero and Sarp 1993) (grey), and the monoclinic cell used in this work (red). The triclinic one refines as a = 10.5455(7) Å, b = 12.6638(5) Å, c = 25.0818(6) Å, α = 89.855(5), β = 89.004(5), γ = 91.953(7)º, the orthorhombic: a = 10.6707(10) Å, b = 6.3284(3) Å, c = 25.0789(8) Å. The powder pattern is represented until 40° 2θ, where the differences are better visible.

FIGURE 6 Zn-OH-CO_3 layer superimposed on the residual electrostatic potential map (difference Fourier map) represented as isosurfaces with levels $\Delta V(r) \geq 3\sigma[\Delta V(r)]$ (yellow), and $\Delta V(r) \geq 2\sigma[\Delta V(r)]$ (white) where hydrogen positions are visible. The map is obtained after a few cycles of dynamical refinement with the incomplete interlayer.

FIGURE 7 Znucalite structure with ZnO_6 octahedra (grey), ZnO_4 tetrahedra (purple), UO_8 hexagonal bipyramids (yellow), CaO_8 (blue) and CO_3 (brown). a) Topology of the $Zn_5(OH)_7(CO_3)$ single-layer. b) (100) and (010) projection of the structure with the composition of the two main layers. Only those hydrogen positions visible from 3D ED data are given.

FIGURE 8 Projections $a \times [0.5–1]b \times [0.65–1.55]c$ representing the U/Ca ordering as observed at the nanoscale from 3D ED and at the powder scale from XRPD. The insert shows a scheme of the fully disordered interlayer for crystals presenting no ordering with $a = a_0$.

FIGURE 9 Rietveld refinement of znucalite from X-ray powder data using the monoclinic settings: a = 10.7655(6) Å, b = 6.3291(2) Å, c = 25.5407(6) Å, β = 100.851(5)º. N_{obs}/N_{all} = 1191/1195, R_{obs}/wR_{obs} = 0.078/0.1063; R_{all}/wR_{all} = 0.0725/0.1063; GOF = 24.51%, R_p = 4.36% and wR_p = 6.22%.

This is the peer-reviewed, final accepted version for American Mineralogist, published by the Mineralogical Society of America.
The published version is subject to change. Cite as Authors (Year) Title. American Mineralogist, in press.
DOI: https://doi.org/10.2138/am-2023-8956. http://www.minsocam.org/

534 **Tables**

535 **Table 1** Selected physical and chemical parameters of the aqueous solutions in contact with
536 znucalite. The temperature in °C, pH, and pe in log units, chemical concentrations in mg/L.
537 Values in parentheses are assumed. Full data is available as a PHREEQC input file in the
538 electronic supplementary information.

sample	**1Cp ZNK**	**Znuk-1**	**ZNU-SE**
temperature	12.0	12.0	12.0
pH	7.02	7.01	6.81
pe	(8.74)	(8.74)	8.74
Cl	554.7	145.6	1967
SO_4	2451	2590	2679
Ag	< BDL	< BDL	0.212
Al	< BDL	< BDL	0.0754
As	< BDL	< BDL	1.027
Ba	0.0299	0.0136	0.102
Ca	407.7	428.8	457.7
Cd	0.0107	0.0265	0.0463
Co	0.0587	0.0794	0.0960
Cu	0.219	0.0846	0.0195
Fe	0.307	< BDL	< BDL
K	550.4	146.8	2132
Li	0.0240	0.0567	0.0999
Mg	301.3	322.6	357.7
Mn	0.0565	0.0140	0.0247
Mo	0.00773	0.0113	0.00893
Na	66.93	58.45	60.18
Ni	21.23	7.093	2.523
Si	10.40	4.823	4.466
Sr	4.649	4.367	4.477
Zn	9.061	20.03	49.89
U	0.504	0.615	0.314

539

540

541

542 **Table 2** Chemical composition (in wt.% oxides) of znucalite from Jáchymov.

Constituent	Mean	Range	Stand. Dev.	Ideal
CaO	3.08	2.76-3.39	0.17	3.08
ZnO	53.09	48.78-54.41	1.28	53.87
Al_2O_3	0.55	0-0.13	0.32	
UO_3	15.14	13.61-16.12	0.72	15.72
SO_3	0.23	0.10-0.52	0.09	
CO_2*	11.56			11.65
H_2O*	15.76			15.68
Total	99.40			100.00

543 CO_2* and H_2O* contents were calculated on the base proposed structural formula and charge
544 balance, ideal composition calculated from structural formula
545 $Zn_{10}Ca_{0.83}(UO_2)_{0.83}(CO_3)_4(OH)_{15.31}(H_2O)_{5.48}$

546

This is the peer-reviewed, final accepted version for American Mineralogist, published by the Mineralogical Society of America.
The published version is subject to change. Cite as Authors (Year) Title. American Mineralogist, in press.
DOI: https://doi.org/10.2138/am-2023-8956. http://www.minsocam.org/

547 **Table 3** 3D ED data collection and crystal structure refinement details for znucalite.

Refined formula	$Zn_{10}Ca_{0.828}[UO_2]_{0.828}[CO_3]_4(OH)_{15.312}(H_2O)_{5.484}$
Unit–cell parameters (3D ED):	
a	10.7215(18) Å
b	6.2592(12) Å
c	25.3550(1) Å
β	101.125(11) °
V	1669.5 (4) $Å^3$
Z	2
Density (for above formula) [$g \cdot cm^{-3}$]	3.003(1)
Space group	$P2_1/m$
Temperature	100 K
TEM	Philips CM120 (data 1), and FEI Tecnai 02 (data 2)
Radiation (wavelength)	electrons (0.0335 Å, and 0.0251 Å)
3D ED technique	Precession-assisted 3D ED
Precession angle	φ = 1 degree
Resolution range (θ)	0.07–1.03
No. of independent reflections (obs/all) – kinematic (merged data)	3901/4466
R_{int} (obs/all) – kinematic	data 1: 0.1538/0.1677; data 2: 0.1647/0.1706
Redundancy (merged)	5.221
Coverage for $\sin\theta/\lambda = 0.713$ $Å^{-1}$ (merged data)	81.33 %
Limiting Miller indices	*h*: –15→ 14, *k*: 0→8, *l*: 0 → 35
Kinematical refinement data 1, 2 in parallel	
No. of reflections (obs/all)	All: 5564/7331 *data 1*: 2035/3364 *data 2*: 3529/3967
R, *wR* (obs); *R*, *wR* (all)	*all*: 0.3296/0.2620; 0.3614/0.2681 *data 1*: 0.2677/0.2085; 0.3816/0.2151 *data 2*: 0.3370/0.3918; 0.3586/0.3970
N refined param.	138
Extinction parameters (Becker Coppens)	*data 2*: *Giso* = 23.33
Dynamical refinement data 1	
No. reflections collected (obs/all)	10459/84270
Coverage for $(sin\theta)/\lambda = 0.725$ $Å^{-1}$	74%
Reflection's selection criteria RSg(max)	0.6
Outlier filtering condition|	*|F(obs)-F(calc)|>15σ(F(obs))*
g(max), No. integration steps,	1.5 $Å^{-1}$, 110 steps
Effective thickness	355(5) Å
No. of reflections (obs/all)	*All:* 3579/20304 *h = 2n: 2700/10212*

	h = 2n +1: 879/10092
No. of filtered reflections	56
R, *wR* (obs)	*All: 0.1594/0.1720*
	h = 2n: 0.1408/0.1554
	h = 2n +1: 0.2448/0.2643
R, *wR* (all)	*All: 0.3677/0.1888*
	h = 2n: 0.2669/0.1644
	h = 2n +1: 0.6016/0.3059
GoF(obs)/GoF(all)	*0.0385/0.0177*
No. of refined param. (structural ones)	244 (148)
Rietveld Refinement against XRPD at the ambient temperature	
No. of reflections (obs/all)	1191/1195
R, *wR* (obs)	0.0718/0.1063
R, *wR* (all)	0.0725/0.1063
No. of refined param. (structural ones)	48
Rp, wRp, GOF	0.0622, 0.0436, 0.2451

548

549

550

This is the peer-reviewed, final accepted version for American Mineralogist, published by the Mineralogical Society of America.
The published version is subject to change. Cite as Authors (Year) Title. American Mineralogist, in press.
DOI: https://doi.org/10.2138/am-2023-8956. http://www.minsocam.org/

551 **Table 4** Bond valence analysis of the Zn-(OH)-CO_3 layer after the dynamical refinement of the
552 incomplete structure of znucalite without the complete interlayer.

atom	*BVS*	*attribution*	*atom*	*BVS*	*attribution*
O1	1.073(16)	$(OH)^-$	O10	0.944(15)	$(OH)^-$
O2	1.03(2)	$(OH)^-$	O1c1	1.84(6)	O^{2-}
O3	1.190(15)	$(OH)^-$	O2c1	2.26(5)	O^{2-}
O4	1.11(2)	$(OH)^-$	O3c1	1.35(4)	O^{2-}
O5	0.991(18)	$(OH)^-$	O1c2	1.73(6)	O^{2-}
O6	1.164(15)	$(OH)^-$	O2c2	2.31(6)	O^{2-}
O7	1.139(14)	$(OH)^-$	O3c2	1.27(5)	O^{2-}
O8	1.178(15)	$(OH)^-$	O1c3	0.328(12)	CO_3
O9	1.30(2)	$(OH)^-$	O1c4	0.57(2)	$CO_3/(OH)^-$

553

554

555 **Table 5** Selected interatomic distances (in Å).

U1−O2c3	2.302(11)	Zn8−O7^{iii}	1.912(7)	C2−O1c2	1.294(12)
U1−O3c3	2.399(10)	Zn8−O1c4	1.919(11)	C2−O2c2	1.297(12)
U1−O1c4	2.483(9)	**<Zn8−O>**	**1.942(9)**	C2−O3c2	1.280(10)
U1−O2c4	2.399(10)	**<Zn−O>$_{tetra}$**	**1.95(1)**	C3−O1c3	1.300(15)
U1−O1c5	2.313(18)	Zn3−O2c1	2.099(7)	C3−O2c3	1.288(11)
U1−O2c5	2.569(12)	Zn3−O1	2.022(8)	C3−O3c3	1.287(14)
<U−O>$_{in-plane}$	2.411(12)	Zn3−O2	2.242(10)	C4−O1c4	1.300(15)
U1−Ou1	1.779(4)	Zn3−O4	2.088(9)	C4−O2c4	1.289(14)
U1−Ou1^{i}	1.779(4)	Zn3−O6	2.046(6)	C4−O3c4	1.276(11)
<U−O>$_{uranyl}$	1.779(4)	Zn3−O8	1.973(6)	C5−O1c5	1.29(3)
Ca1−O11	2.662(17)	**<Zn3−O>**	**2.078(8)**	C5−O2c5	1.29(2)
Ca1−O1ca1	2.358(12)	Zn4−O2c2	2.183(8)	C5−O3c5	1.28(2)
Ca1−O3ca1	2.250(12)	Zn4−O1 ^{iv}	2.059(9)	**<C−O>**	**1.29(2)**
Ca1−O2ca1	2.777(18)	Zn4−O6 ^{iv}	1.923(8)	O1−H1o1	1.000(17)
Ca1−O2ca1^{i}	2.777(18)	Zn4−O6 ^{iii}	1.923(8)	O2−H1o2	1.00(2)
Ca1−O3ca1^{i}	2.250(12)	Zn4−O7	2.215(8)	O3−H1o3	1.00(2)
Ca1−O2c4	2.251(13)	Zn4−O7^{i}	2.215(8)	O4−H1o4	1.00(2)
Ca1−O2c5	2.478(14)	**<Zn4−O>**	**2.086(8)**	O5−H1o5	1.00(3)
<Ca−O>	**2.475(2)**	Zn5−O2c2	2.240(7)	O6−H1o6	1.01(3)
Zn1−O1c2	2.018(10)	Zn5−O3^{vi}	2.112(6)	O7−H1o7	1.00(2)
Zn1−O2	1.867(10)	Zn5−O5	2.081(9)	O8−H1o8	1.00(1)
Zn1−O3	1.802(7)	Zn5−O7	2.180(6)	O9−H1o9	1.00(2)
Zn1−O3^{i}	1.802(7)	Zn5−O9	1.988(8)	O10−H1o10	1.00(2)
<Zn1−O>	**1.872(9)**	Zn5−O10	2.152(8)	O3c1−H1o2^{ii}	1.76(3)
Zn2−O1c1	1.903(10)	**<Zn5−O>**	**2.126(7)**	O1c1−H1o3	2.40(3)
Zn2−O5	2.099(11)	Zn7−O2c1	2.097(8)	O1c1−H1o3^{v}	2.40(3)
Zn2−O6^{ii}	2.099(7)	Zn7−O3	2.258(8)	O2c3−H1o4	1.73(2)
Zn2−O6^{iii}	2.099(7)	Zn7−O3^{v}	2.258(8)	O3c2−H1o5^{vii}	1.71(3)
<Zn2−O>	**2.05(1)**	Zn7−O8	2.135(8)	O3c1−H1o6	1.67(2)
Zn6−O1c3	2.174(12)	Zn7−O8^{v}	2.135(8)	O3c1−H1o6^{v}	1.67(2)
Zn6−O8	1.945(7)	Zn7−O10^{viii}	2.015(9)	Ow2−H1o7^{ii}	1.74(4)
Zn6−O8^{i}	1.945(7)	**<Zn7−O>**	**2.150(8)**	Ow2−H1o7^{iii}	1.74(4)
Zn6−O9^{vii}	1.863(11)	**<Zn−O>$_{octa}$**	**2.110(8)**	Ow2b−H1o7^{ii}	1.80(3)
<Zn6−O>	**1.982(9)**	C1−O1c1	1.289(13)	Ow2b−H1o7^{iii}	1.80(3)
Zn8−O4	2.024(10)	C1−O2c1	1.284(12)	Ow1−H1o8	2.34(2)
Zn8−O7^{iv}	1.912(7)	C1−O3c1	1.282(10)	Ow1−H1o8^{v}	2.34(2)

O3c4–H1o9^{iv}	2.15(2)

(i) x,-y+3/2,z; (ii) -x+1,y-1/2,-z+1; (iii) -x+1,-y+1,-z+1; (iv) -x+1,y+1/2,-z+1; (v) x,-y+1/2,z; (vi) -x+2,-y+1,-z+1; (vii) -x+2,y+1/2,-z+1; (viii) -x+2,y-1/2,-z+1; (ix) -x+1,y+1/2,-z+2; (x) -x+1,-y+1,-z+2; (xi) x+1,y,z.

This is the peer-reviewed, final accepted version for American Mineralogist, published by the Mineralogical Society of America.
The published version is subject to change. Cite as Authors (Year) Title. American Mineralogist, in press.
DOI: https://doi.org/10.2138/am-2023-8956. http://www.minsocam.org/

analysis of znucalite crystal structure (in *v.u.*) (without hydrogen contribution)

Zn2	Zn3	Zn4	Zn5	Zn6	Zn7	Zn8	Ca1	C1	C2	C3	C4	C5	sum	Assignment
0.56								1.31					1.87	O
	0.34				0.34			1.33					2.01	O
								1.34					1.34	O
									1.30				1.72	O
		0.27	0.23						1.29				1.79	O
									1.35				1.35	O
				0.28						1.28			1.56	O
										1.32			1.80/1.32	O
										1.32			1.71/1.32	O
						0.54					→0/1.28 ↓1.28		0.54/2.2	OH/O
							0.42				1.31		2.2	O
											1.36		1.36	O
												→0/1.31 ↓1.31	0.54/1.88	OH/O
							0.24					→0/1.3 ↓1.30	0.57/1.87	OH/O
												1.35	1.35	O
													1.76	O
	0.41	0.38											1.20	OH
	0.23												1.09	OH
			0.33		→0.225 ↓0.45								1.29	OH
	0.35					0.41							1.11	OH
0.34			0.35										1.05	OH
→0.34 ↓0.68	0.39	→0.54 ↓1.07											1.265	OH
		→0.25 ↓0.5	0.27			→0.55 ↓1.1							1.07	OH
	0.47			→0.55 ↓1.01	→0.31↓0.62								1.33	OH
			0.45	0.63									1.08	OH
			0.29		0.42								0.71	OH

This is the peer-reviewed, final accepted version for American Mineralogist, published by the Mineralogical Society of America.
The published version is subject to change. Cite as Authors (Year) Title. American Mineralogist, in press.
DOI: https://doi.org/10.2138/am-2023-8956. http://www.minsocam.org/

Ow2																0.00	H_2O
Ow1b																0.00	H_2O
Ow2b																0.00	H_2O
O11										0.15						0.15	H_2O
O1ca1										0.32						0.32	H_2O
O2ca1										0.12						0.12	H_2O
O3ca1										0.43						0.43	H_2O
sum	6.34	2.51	1.58	2.19	2.22	1.94	1.92	1.82	2.06	1.68	3.98	3.93	3.91	3.95	3.95		

All values given in the valence-units (vu); the analysis was undertaken following the procedure of Brown (2002) using the bond-valence parameters givem by Gagné and Hawthorne (2015).

Table 7 Hydrogen contribution to the Bond valence analysis of znucalite crystal structure (in *v.u.*)

atom	sum	Assignment	H	Sum with H	atom	sum	Assignment	H	Sum with H
O1c1	1.87	O		1.87	O2	1.09	OH	+0.8	1.89
O2c1	2.01	O		2.01	O3	1.29	OH	+0.8	2.09
O3c1	1.34	O	+0.4	1.74	O4	1.11	OH	+0.8	1.91
O1c2	1.72	O		1.72	O5	1.05	OH	+0.8	1.85
O2c2	1.79	O		1.79	O6	1.265	OH	+0.8	2.065
O3c2	1.35	O	+0.6	1.95	O7	1.07	OH	+0.8	1.87
O1c3	1.56	O		1.56	O8	1.33	OH	+0.8	2.13
O2c3	1.80/1.32	O	+0.2	2/1.52	O9	1.08	OH	+0.8	1.88
O3c3	1.71/1.32	O		1.71/1.32	O10	0.71	OH	+0.8	1.51
O1c4	0.54/2.2	OH/O	+0.8/0	1.34/2.2	Ow1	0.00	H_2O	+1.6	1.6
O2c4	2.2	O		2.2	Ow2	0.00	H_2O	+0.4+1.6	2
O3c4	1.36	O	+0.2	1.56	Ow1b	0.00	H_2O	+1.6	1.6
O1c5	0.54/1.88	OH/O	+0.8/0	1.34/1.88	Ow2b	0.00	H_2O	+0.4+1.6	2
O2c5	0.57/1.87	OH/O	+0.8/0	1.37/1.87	O11	0.15	H_2O	+1.6	1.75
O3c5	1.35	O		1.35	O1ca1	0.32	H_2O	+1.6	1.92
Ou1	1.76	O		1.76	O2ca1	0.12	H_2O	+1.6	1.72
O1	1.20	OH	+0.8	2	O3ca1	0.43	H_2O	+1.6	2.03

563 **Table 8** Unit-cell parameters reported and determined during this study (3D ED at 100K and
564 XRPD at the ambient temperature) for znucalite and related phases compared to the literature
565 data.

Different indexings	*a* (Å)	*b* (Å)	*c* (Å)	α (º)	β (º)	γ (º)
Orthorhombic (Chiappero and Sarp 1993)	10.72(1)	25.16(1)	6.325(4)	90	90	90
Triclinic (Ondruš et al. 1990)	12.692(4)	25.096(6)	11.685(3)	89.08(2)	91.79(2)	90.37(3)
Monoclinic (this work, XRPD) P2_1*/m*	10.7655(6)	6.3291(2)	25.5407(6)	90	100.851(5)	90
Monoclinic (3D ED, 100K) P2_1*/m*	10.7215(18)	6.2592(12)	25.3550(1)	90	101.125(11)	90
Basic cell; disordered model (3D ED, 100K)	5.311(1)	6.3291(2)	25.099(1)	90	92.032(1)	90
Pseudo-orthorhombic (this work, SC-XRD, room temp.)	5.3807(16)	6.3273(13)	25.129(12)	90	90.59(3)	90
Related mineral and synthetic compounds						
$Zn_5(OH)_{10}\cdot 2H_2O$ *C*2/*c* (Gordeeva et al. 2020)	15.342(7)	6.244(6)	10.989(7)	90	100.86(1)	90
Hydrozincite, $Zn_5(OH)_6(CO_3)_2$, *C*2/*m* (Ghose 1964)	13.62	6.30	5.42	90	95.5	90
$Zn_5(OH)_8(NO_3)_2\cdot 2H_2O$ *C*2/*m* (Stählin and Oswald 1970)	19.480(5)	6.238(1)	5.517(1)	90	93.28(1)	90
Aurichalcite $(Cu,Zn)_5(OH)_6(CO_3)_2$, *P*2_1*/m* (Harding et al. 1994)	13.82(2)	6.419(3)	5.29(3)	90	101.04(2)	90

566

This is the peer-reviewed, final accepted version for American Mineralogist, published by the Mineralogical Society of America.
The published version is subject to change. Cite as Authors (Year) Title. American Mineralogist, in press.
DOI: https://doi.org/10.2138/am-2023-8956. http://www.minsocam.org/

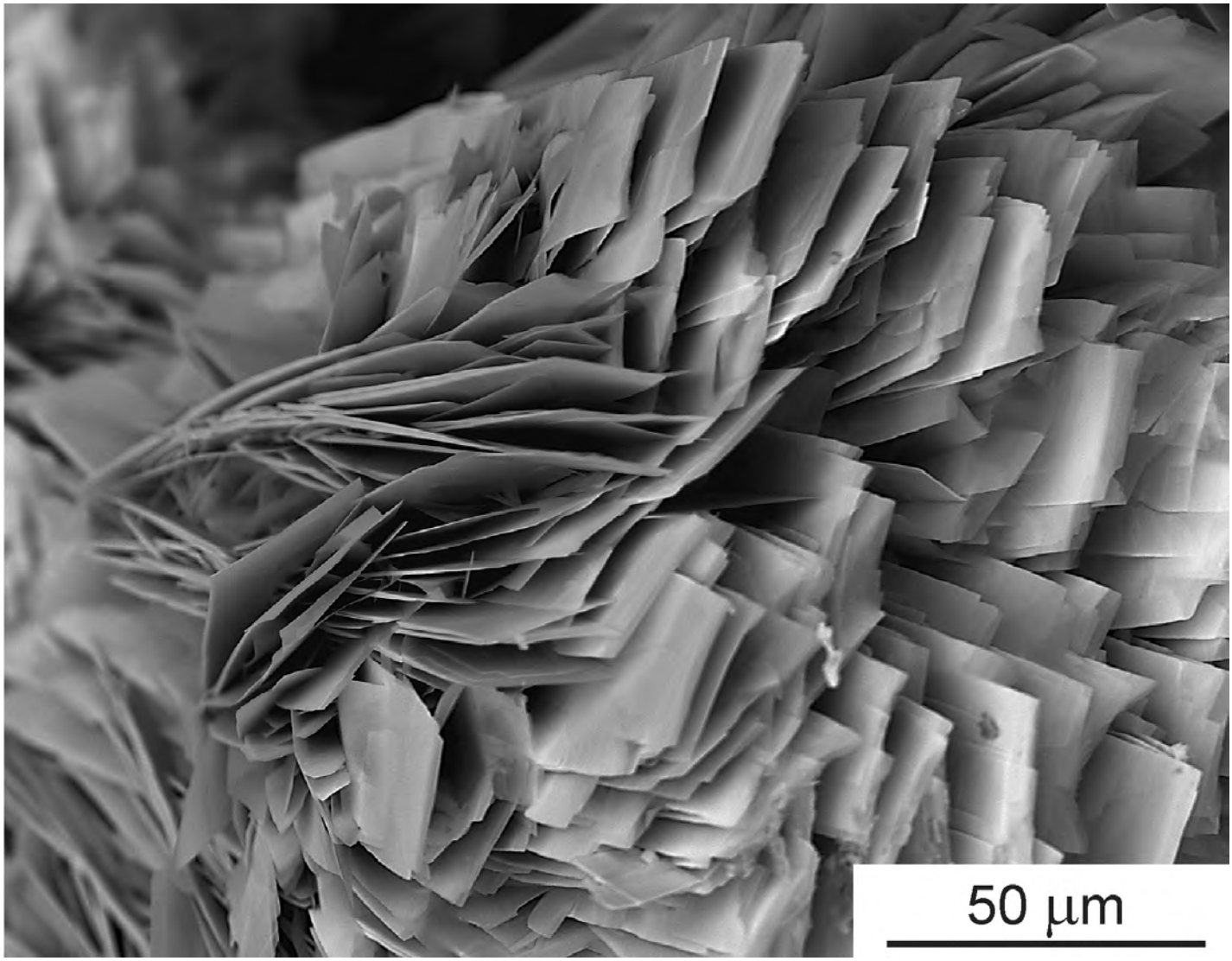

1

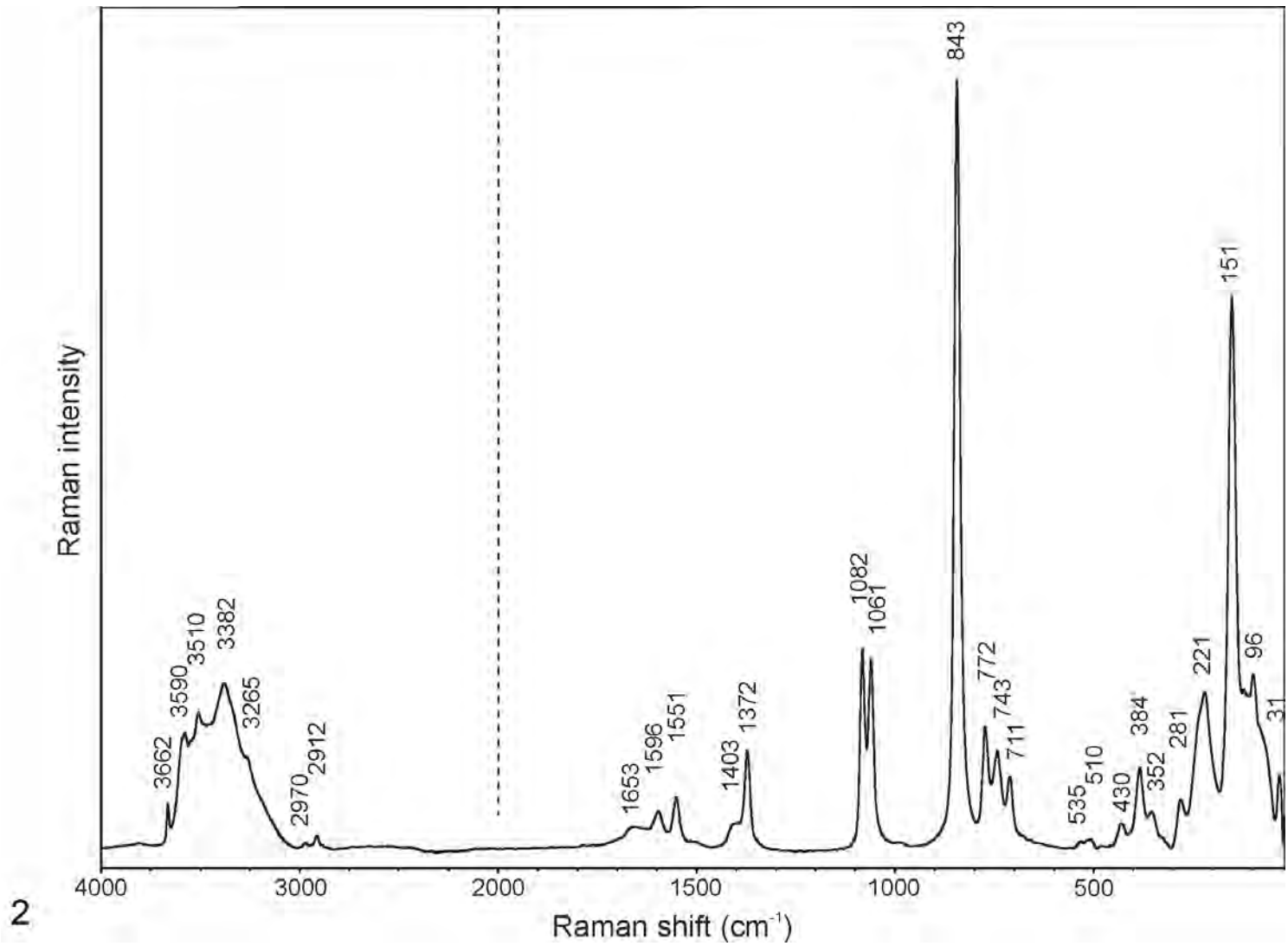

2

This is the peer-reviewed, final accepted version for American Mineralogist, published by the Mineralogical Society of America.
The published version is subject to change. Cite as Authors (Year) Title. American Mineralogist, in press.
DOI: https://doi.org/10.2138/am-2023-8956. http://www.minsocam.org/

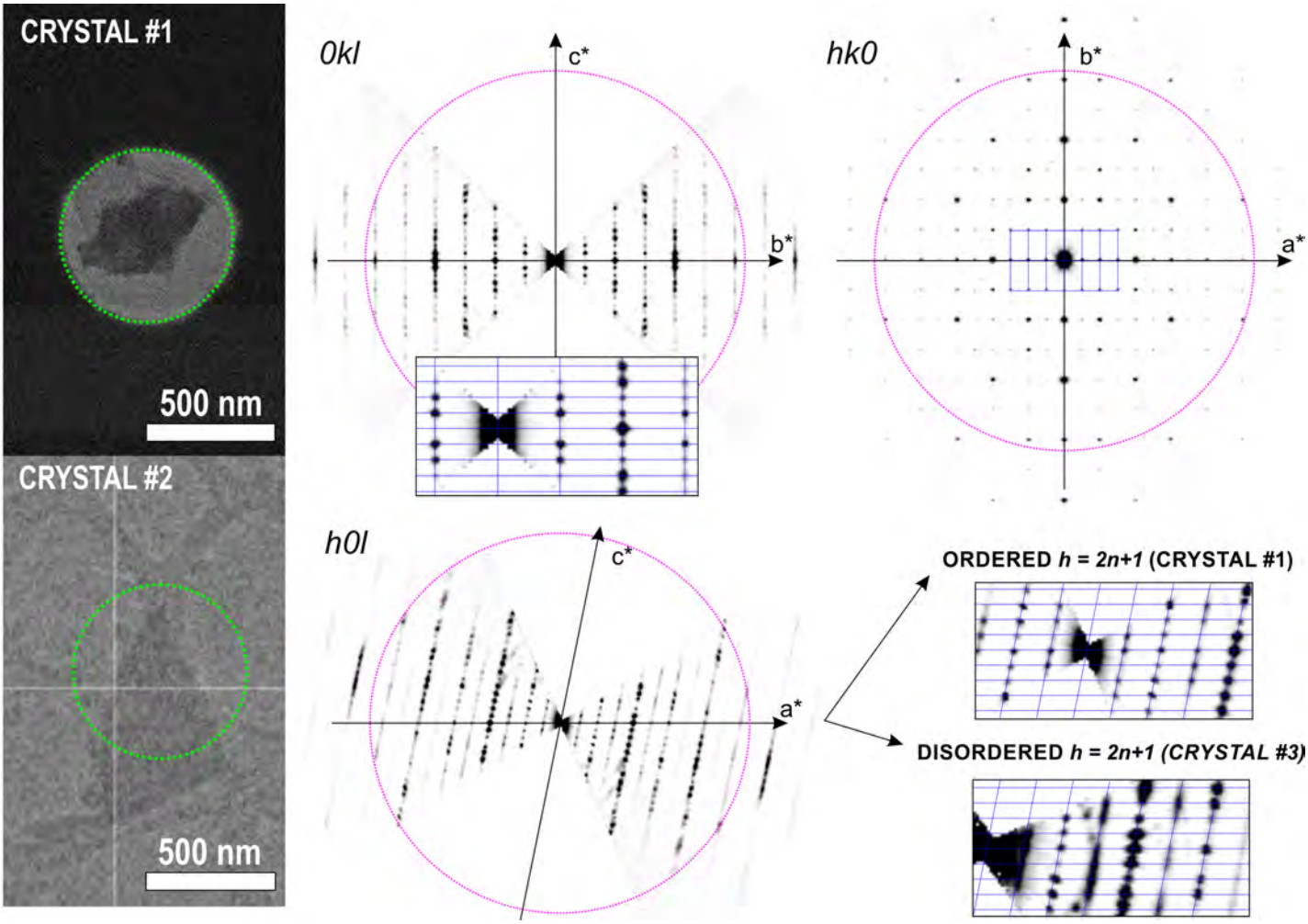

This is the peer-reviewed, final accepted version for American Mineralogist, published by the Mineralogical Society of America.
The published version is subject to change. Cite as Authors (Year) Title. American Mineralogist, in press.
DOI: https://doi.org/10.2138/am-2023-8956. http://www.minsocam.org/

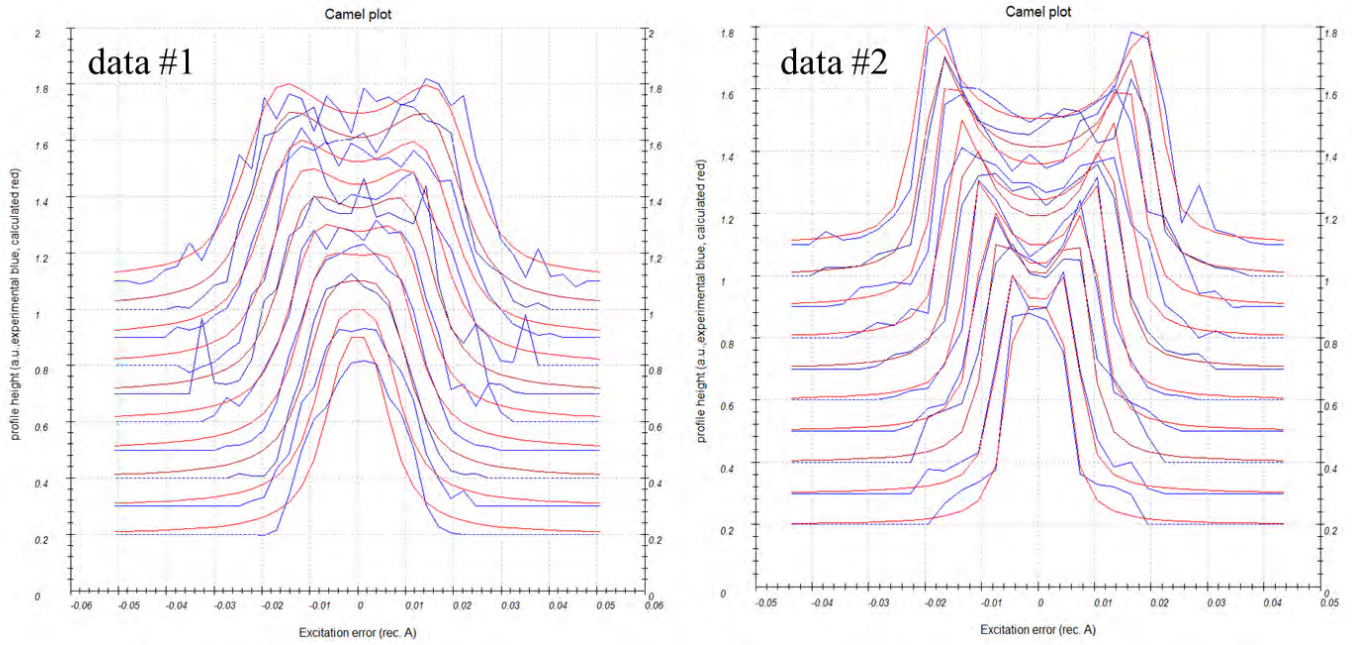

4

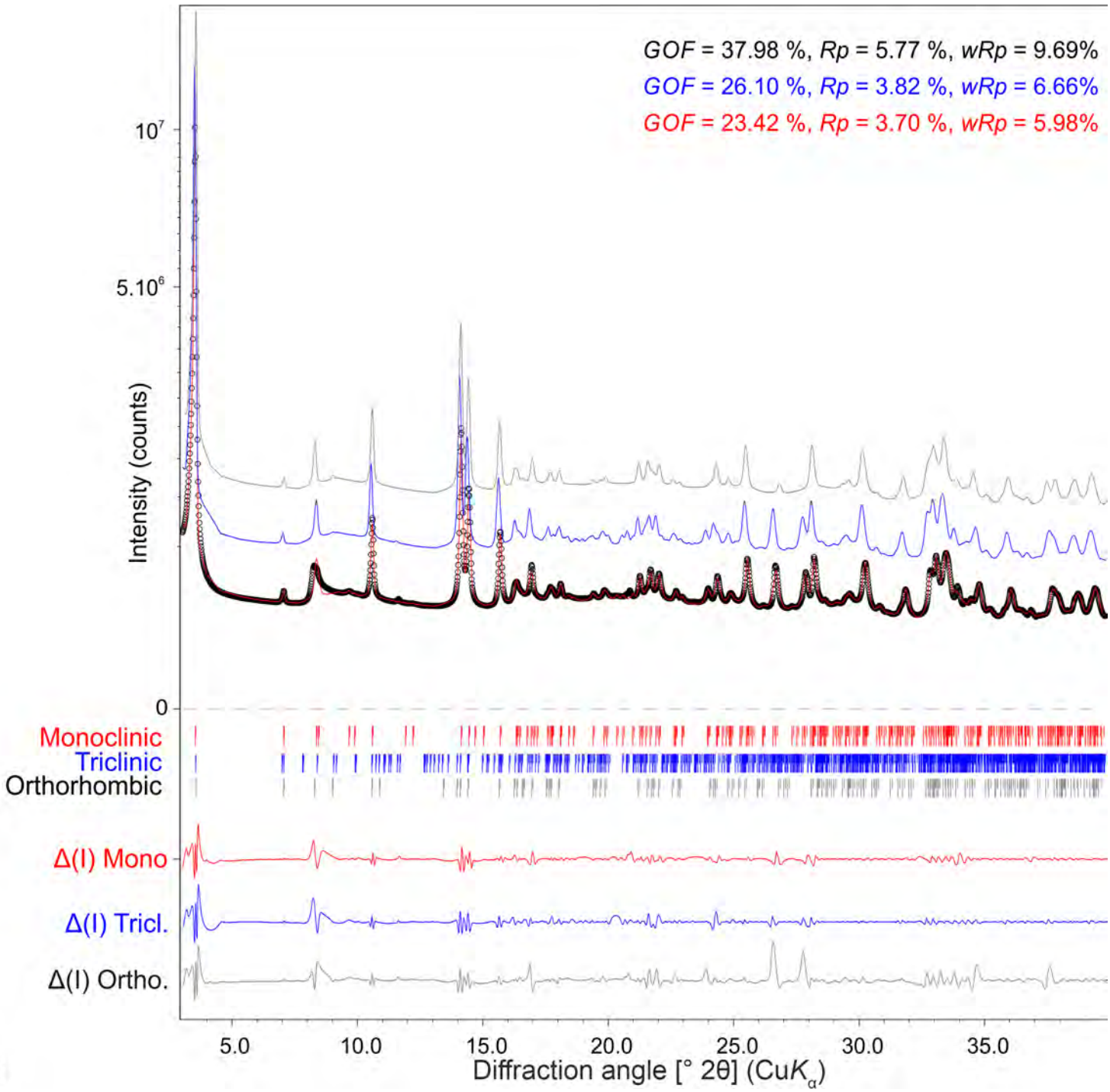

This is the peer-reviewed, final accepted version for American Mineralogist, published by the Mineralogical Society of America.
The published version is subject to change. Cite as Authors (Year) Title. American Mineralogist, in press.
DOI: https://doi.org/10.2138/am-2023-8956. http://www.minsocam.org/

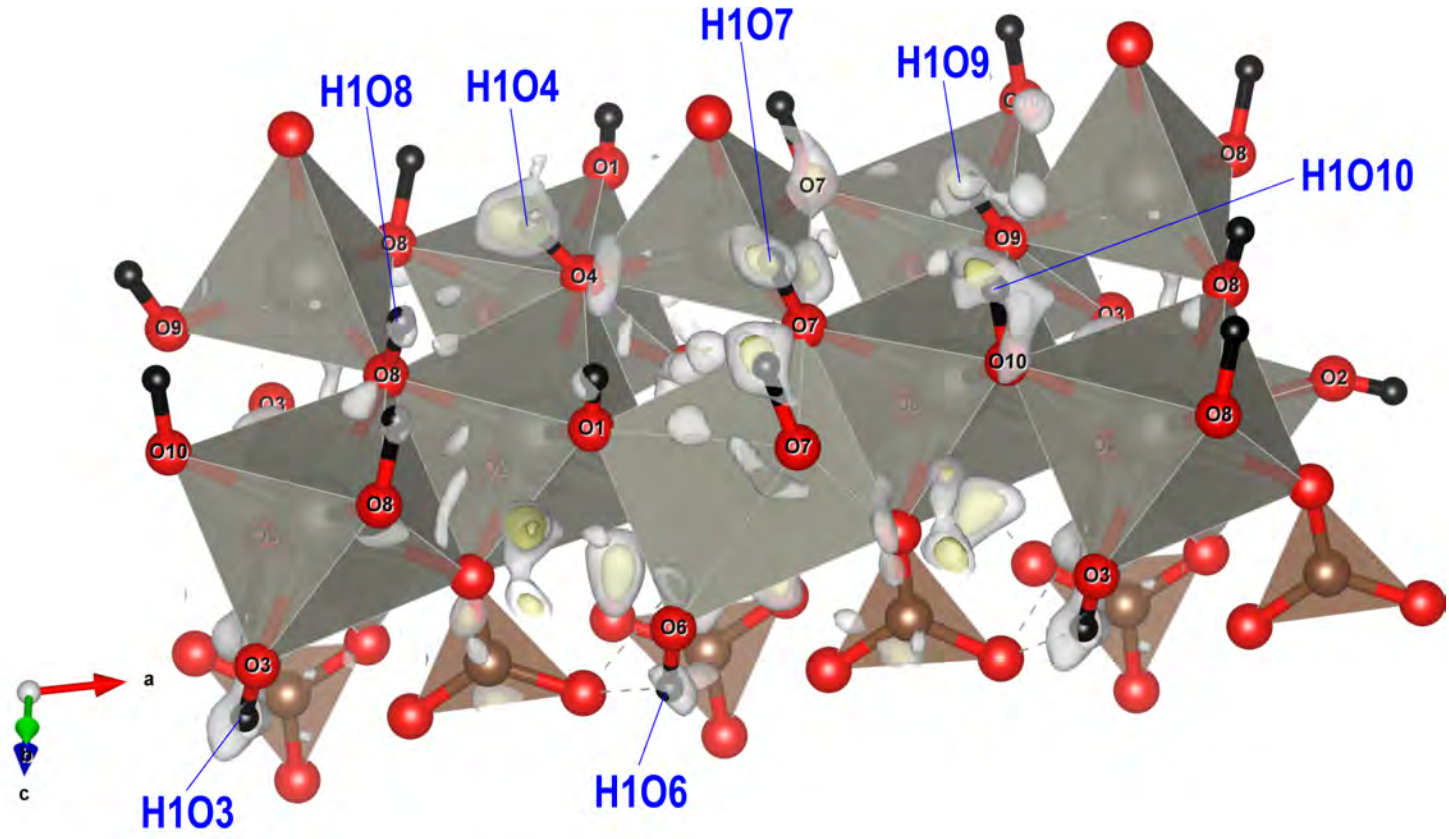

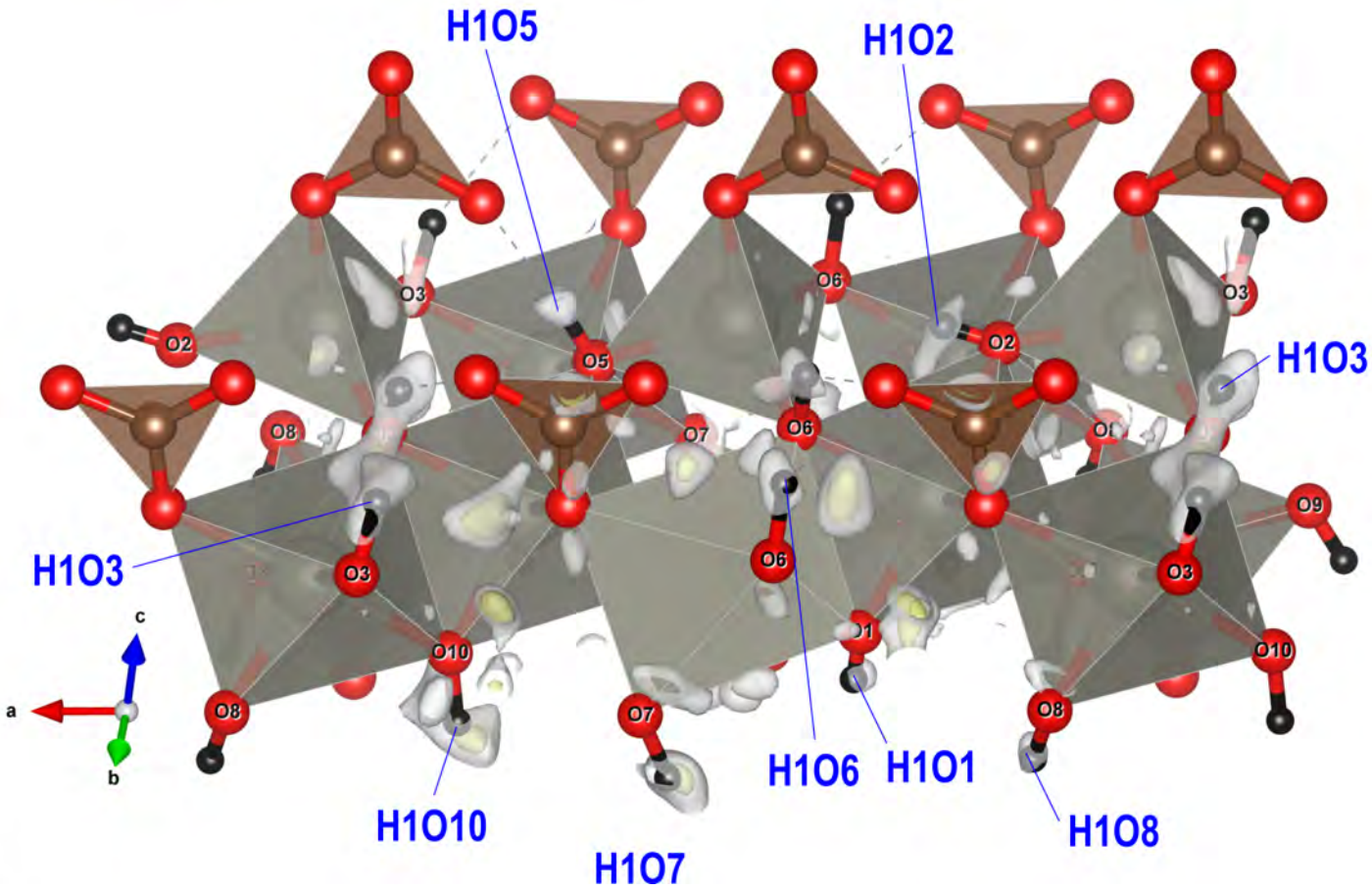

This is the peer-reviewed, final accepted version for American Mineralogist, published by the Mineralogical Society of America.
The published version is subject to change. Cite as Authors (Year) Title. American Mineralogist, in press.
DOI: https://doi.org/10.2138/am-2023-8956. http://www.minsocam.org/

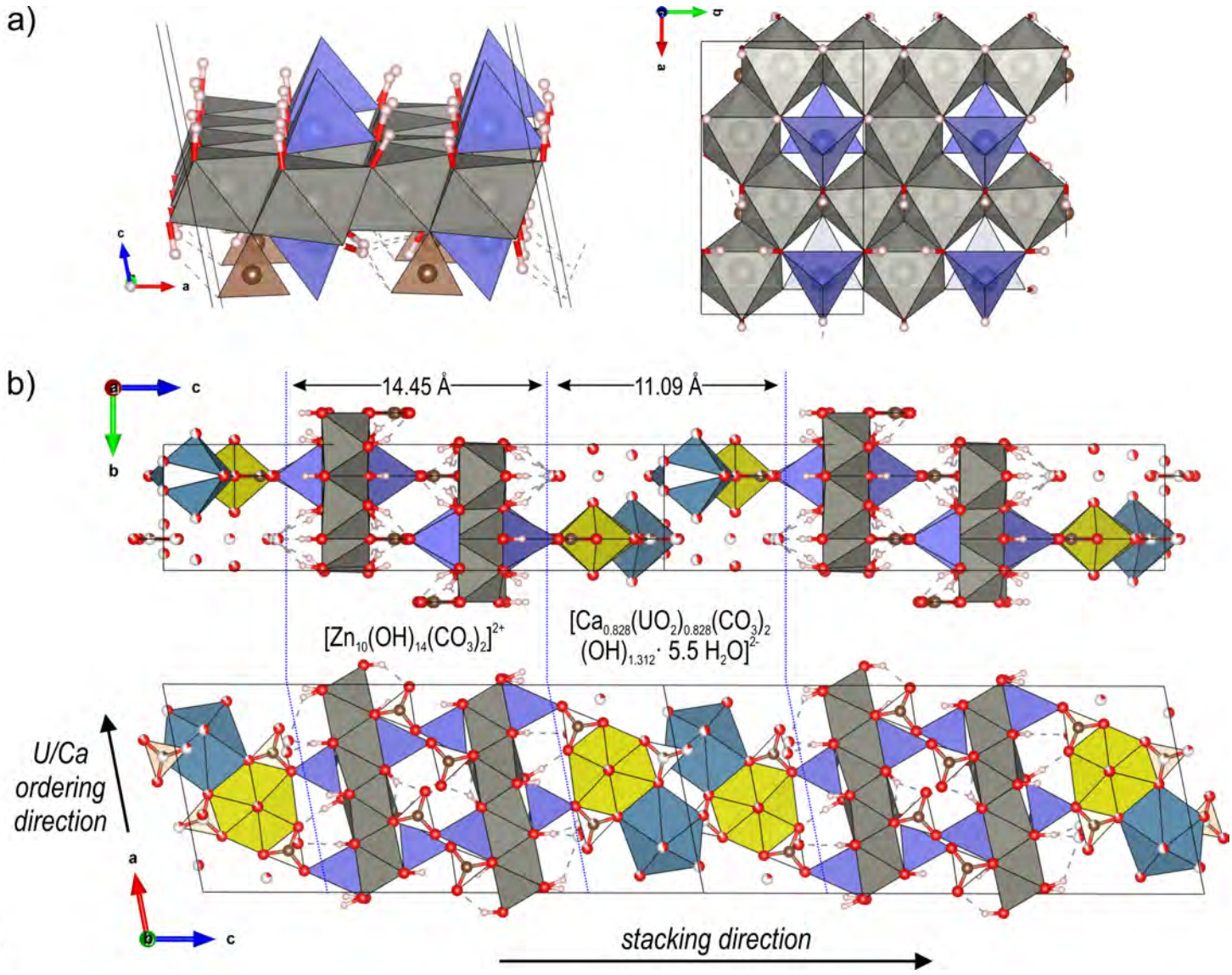

7

This is the peer-reviewed, final accepted version for American Mineralogist, published by the Mineralogical Society of America.
The published version is subject to change. Cite as Authors (Year) Title. American Mineralogist, in press.
DOI: https://doi.org/10.2138/am-2023-8956. http://www.minsocam.org/

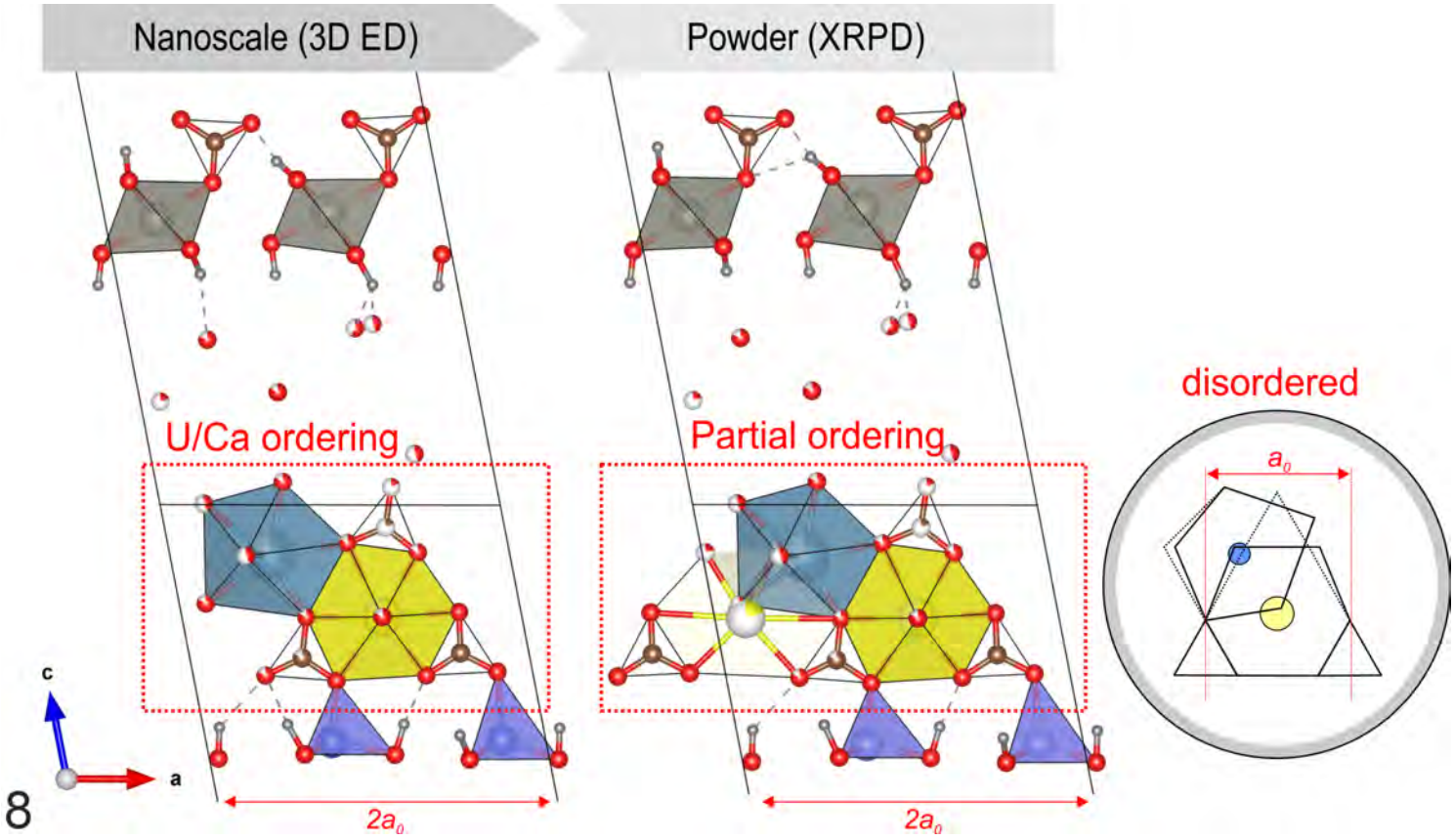

8

This is the peer-reviewed, final accepted version for American Mineralogist, published by the Mineralogical Society of America.
The published version is subject to change. Cite as Authors (Year) Title. American Mineralogist, in press.
DOI: https://doi.org/10.2138/am-2023-8956. http://www.minsocam.org/

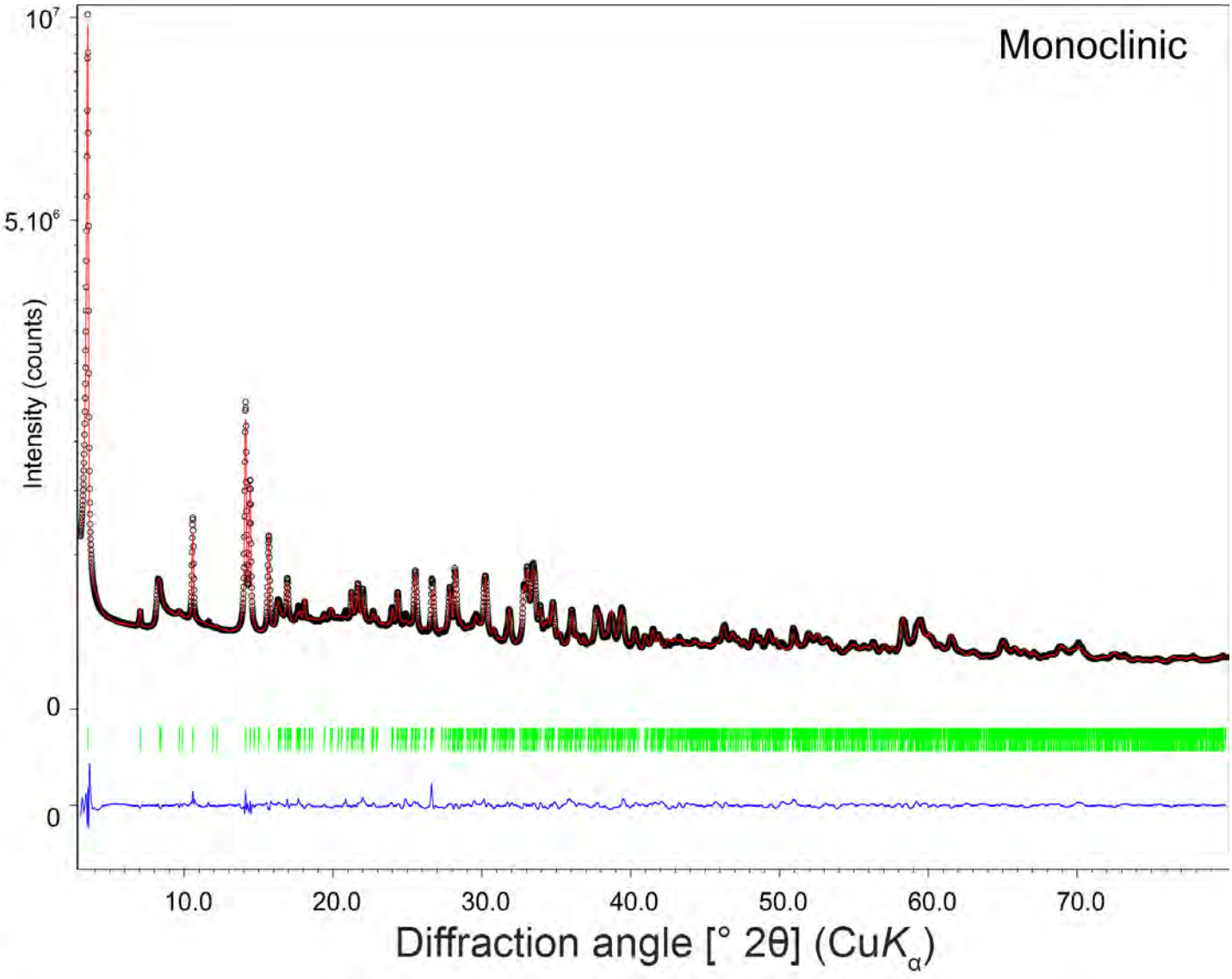

9